Atomistic model of gallium

M. I. Baskes, S. P. Chen, and F. J. Cherne
Los Alamos National Laboratory, Los Alamos, New Mexico 87545
(Received 26 September 2001; revised manuscript received 22 January 2002; published 27 September 2002)

A modified embedded atom model of gallium has been developed. This simple atomic level model is able to reproduce the unusual behavior of this complex element. The calculated energetics and volumes of many allotropic phases of gallium are found to be in close agreement with first principles calculations and experiment. Calculated thermodynamic and elastic properties are also in reasonable agreement with the available experimental and first principles data. The model also reproduces the low melting point of gallium.

DOI: 10.1103/PhysRevB.66.104107 PACS number(s): 61.50.Lt, 61.72.Ji, 62.20.Dc, 64.70.Dv

I. INTRODUCTION

Gallium is a very complex element. Its compounds are of extreme importance in the electronics industry. The gallium phase diagram shows the existence of one equilibrium solid phase A11 (oC8, GaI) as well as the liquid phase at atmospheric pressure and three additional equilibrium phases face centered tetragonal (fct) (cI12, GaII), A6 (tF4, tI2, GaIII), and fcc (GaIV) at high pressure.[1] We present the structures in various crystallography nomenclatures to aid the reader. In addition a number of metastable phases are also readily formed at pressures around 10 GPa. One of the metastable phases, β-Ga (mC4), is essentially the same structure as the A20 (oC4) structure. The equilibrium phase at low pressure is the orthorhombic A11 phase. This phase shows a significant amount of dimerization. The melting point of gallium is only slightly greater than room temperature (303 K).

The embedded atom method (EAM), which is based on density functional theory, is by far the most widely used semiempirical atomistic method. Applications of the EAM include calculation of properties of perfect and defective (free surfaces, point defects, grain boundaries, dislocations, etc.) bulk metals and alloys as a function of temperature and pressure. Recent research has led to models of similarly complex elements, tin[2] and plutonium.[3] These models were based on the EAM (Refs. 4–6) which has been found to represent the properties of metals and alloys quite well. In the work on tin it was found that the model was able to quantitatively predict the thermodynamics of the three equilibrium phases of tin. The addition of angular forces[7] was found to be critical in explaining the behavior of complex crystal structures. Thus the modified EAM (MEAM) (Refs. 7–9) is used here to model the properties of gallium.

One may question why are we interested in semiempirical models when first-principles calculations have progressed to a high level of accuracy. The issue is simply practicality. For obtaining an understanding of complex phenomena in physics or materials science, many thousands of atoms are required to simulate the relevant processes. In addition, the desire to calculate statistical or thermodynamic properties obviates the calculation of millions of energies. Unfortunately first-principles calculations are just too slow to be useful for these problems. Thus we are reduced to developing simple models which mimic the real world. The challenge presented here is whether or not a simple model such as the MEAM can sufficiently represent a complex material such as gallium so as to be useful.

The models of tin and plutonium used experimental data as input to the MEAM model. For the case of gallium, first principles calculations were used to develop the database required to determine the properties of the MEAM model.

II. THEORY

A. Details of the model

The total energy E of a system of monatomic atoms in the EAM formalism is[4–6] given by an expression of the form,

$$E=\sum_i \left(F(\overline{\rho}_i)+\frac{1}{2}\sum_{j\neq i}\phi(R_{ij})\right), \tag{1}$$

where the indices i and j denote the atoms. The embedding function F is the energy to embed an atom into the background electron density at site i, $\overline{\rho}_i$; and ϕ is the pair interaction between atoms i and j whose separation is given by R_{ij}. In the EAM, $\overline{\rho}_i$ is given by a linear supposition of spherically averaged atomic electron densities, while in the Modified Embedded Atom Method (MEAM), $\overline{\rho}_i$ has an angular dependence.[7–9]

The pair potential between two atoms $\phi(R)$ separated by a distance R is given by

$$\phi(R)=\frac{2}{Z}\{E^u(R)-F(\overline{\rho}^0(R))\}, \tag{2}$$

where $\overline{\rho}^0(R)$ is the background electron density at an atom in what is termed the reference structure, and Z is the number of first neighbors in this structure. Here $E^u(R)$ is the energy per atom of the reference structure as a function of nearest neighbor distance R, obtained, e.g., from first principles calculations or the universal equation of state of Rose *et al.*,[10]

$$E^u(R)=-E_c\left(1+a^*+\frac{r_e}{R}\delta a^{*3}\right)e^{-a^*} \tag{3}$$

with

$$a^*=\alpha\left(\frac{R}{r_e}-1\right) \tag{4}$$

and

$$\alpha^2 = \frac{9\Omega B}{E_c}, \tag{5}$$

where E_c, r_e, Ω, and B are the cohesive energy, nearest-neighbor distance, atomic volume, and bulk modulus, respectively, all evaluated at equilibrium in the reference structure. The parameter δ has been added to better represent the pressure derivative of the bulk modulus. In this work the reference structure will be taken as the fcc, resulting in

$$\overline{\rho}^0(R) = Z\rho^{a(0)}(R), \tag{6}$$

where $\rho^{a(0)}$ is an atomic electron density discussed below and $Z=12$ is the number of nearest neighbors in the reference structure.

In the MEAM the embedding function $F(\overline{\rho})$ is taken as

$$F(\overline{\rho}) = AE_c \frac{\overline{\rho}}{Z} \ln \frac{\overline{\rho}}{Z}, \tag{7}$$

where A is an adjustable parameter.

The background electron density at a specific site, $\overline{\rho}$, is assumed to be a function of what we call partial electron densities. These partial electron densities contain the angular information in the model. The spherically symmetric partial electron density $\rho^{(0)}$ is the background electron density in the EAM,

$$\rho^{(0)} = \sum_{j \neq i} \rho^{a(0)}(R_{ij}), \tag{8}$$

where the sum is over all atoms j not including the atom at i. The angular contributions to the density are given by similar formulas weighted by the x, y, and z projections of the distances between atoms[11] (see the Appendix for the detailed formulas). The atomic electron densities are given by simple exponentials with decay constant $\beta^{(l)}$, $l=0-3$. To obtain the background electron density from the partial electron densities we make the assumption that the angular terms are a small correction to the EAM. We combine the angular dependence into one term,

$$\Gamma = \sum_{l=1}^{3} t^{(l)} (\rho^{(l)}/\rho^{(0)})^2, \tag{9}$$

where the $t^{(l)}$ are constants. The background density is then taken as

$$\overline{\rho} = \rho^{(0)} \sqrt{1+\Gamma}. \tag{10}$$

It has been shown that this formalism is equivalent to an expansion of the background electron density in Legendre polynomials.[7,12]

B. First principles method

The first principles calculations were performed to provide some physical properties of the fcc, hcp, simple cubic (sc), bcc, and A11 phases of Ga. Some of these quantities are not readily available from experiment. These first principles calculations were performed to insure that the fitted MEAM Ga potentials are sufficiently transferable for a wide variety of modeling and simulation environments.

TABLE I. Source and values of MEAM parameters for gallium.

Parameter	Source	Value
E_c (eV/atom)	cohesive energy of fcc (GGA)	2.897
r_e (Å)	lattice constant of fcc (GGA)	4.247
α	bulk modulus of fcc (GGA)	4.42
δ	energy/volume curve of fcc (GGA)	0.097
A	relative energy of sc and fcc (GGA)	0.97
$\beta^{(0)}$	volume per atom of A11 (GGA)	4.80
$\beta^{(1)}$	force on atom near vacancy in fcc (GGA)	3.10
$\beta^{(2)}$	shear modulus fcc (GGA)	6.00
$\beta^{(3)}$	relative energy of fcc and A11 (GGA)	0.50
$t^{(1)}$	vacancy formation energy in fcc (GGA)	2.72
$t^{(2)}$	shear modulus fcc (GGA)	2.06
$t^{(3)}$	relative energy of fcc and hcp (GGA)	−4.00
$c_{\min}$	thermal expansion (experiment)	1.40

We have used the ultrasoft (US) pseudopotential[13] of Ga with the generalized gradient approximation (GGA) (Ref. 14) to the exchange-correlation energy using the VASP code.[15,16] The $3d10$, $4s2$, $4p$ electrons are treated as valence electrons (total of 13 electrons). For the fcc structure, we used $20\times20\times20$ Monkhorst-Pack[17] k-point mesh in the primitive cell. For the bcc, sc, A4, A6, A11, and hcp structure, a $16\times16\times16$, $16\times16\times16$, $8\times8\times8$, $10\times10\times10$, $8\times8\times8$, and $6\times6\times6$ k-point mesh was used, respectively.

The vacancy formation energy, without any structural relaxations, in a 32-atom fcc-cell was calculated so the defect energy can be calibrated for the MEAM. The formula for the vacancy formation energy is

$$E_f^{1v} = E_{31} - (31/32)E_{32}, \tag{11}$$

where E_N is the energy of an N-atom unit cell.

C. Obtaining the model parameters

The MEAM parameters are obtained by using first principles data for gallium with a reference lattice of the fcc. In Table I the source of the first principles quantity and the resultant parameter value is given. The data used includes the cohesive energy E_c, the lattice constant a, the force on a neighbor to an unrelaxed vacancy, f_v, and the elastic constants c_{ij} of the fcc gallium. In addition, the energies of structures $X=$ sc, hcp, and A11 gallium relative to fcc gallium, ΔE_X and the volume of A11 gallium Ω_{A11} were used. E_c, α, δ, and $r_e = a/\sqrt{2}$ are determined by least squares fitting to the energy vs volume obtained from the GGA calculations. To obtain A, the following equation is used:

$$A = \frac{-E_c + \delta E_{\mathrm{sc}} + 0.5E_c(1+a_{\mathrm{sc}}^*)e^{-a_{\mathrm{sc}}^*}}{0.5E_c \ln(0.5) e^{-b_{\mathrm{sc}}^*}}, \tag{12}$$

where

$$a_{\mathrm{sc}}^* = \alpha(x_{\mathrm{sc}} - 1), \tag{13}$$

$$b^*_{sc} = \beta^{(0)}(x_{sc} - 1), \tag{14}$$

and the ratio of nearest distances in the sc structure to the fcc structure is given by

$$x_{sc} = \frac{\sqrt{2}}{4^{1/3}}. \tag{15}$$

An iterative procedure was used to calculate $\beta^{(0)}$, using the volume of the A11 structure. The force on a neighbor to an unrelaxed vacancy is used to calculate $\beta^{(1)}$. The analytic equation giving this relationship is given in the Appendix (see Baskes *et al.*[11] for the derivation). The elastic constants of the fcc phase are used to determine $\beta^{(2)}$ and $t^{(2)}$ using equations presented in the Appendix which were derived from Baskes.[7] It was found that no value of $\beta^{(2)}$ reproduced the GGA elastic constant $c'_{12}=0.5$ $(c_{11}-c_{12})$ and the GGA energy of the A11 phase simultaneously. The best agreement was found by choosing $\beta^{(2)}=6$. The relative energy of A11 and fcc is used to determine $\beta^{(3)}$ under the constraint of wanting a reasonably good value of c'_{12}. An iterative process is employed, as no simple analytic formula is available. The hcp/fcc relative energy is used to determine $t^{(3)}$ and the vacancy formation energy is used to determine $t^{(1)}$ using equations presented in the Appendix which were taken from Baskes.[7]

Even though the parameters are not completely uncorrelated, there is a very close connection between each piece of experimental data and the resultant parameter. Angular screening was implemented (see the Appendix) using the values, $C_{min}=1.4$ and $C_{max}=2.8$, as in the method of Baskes *et al.*[18] As shown in Baskes[19] the choice of C_{min} strongly effected the thermal expansion. Thus we determine C_{min} by fitting to the experimental value for the thermal expansion coefficient. For computational convenience, a radial cutoff of 5.0 Å was also used.[19]

The procedure of parameterization may be summarized as follows:

(1) E_c, α, δ, and $r_e = a/\sqrt{2}$ are determined by least squares fitting to the fcc energy vs volume obtained from the GGA calculations;
(2) A is determined from Eq. (12) using the properties of the sc phase;
(3) An iterative process is used to calculate $\beta^{(0)}$, using the volume of the A11 structure;
(4) The force on a neighbor to an unrelaxed vacancy is used to calculate $\beta^{(1)}$ using Eqs. (A5);
(5) The elastic constants of the fcc phase are used to determine $\beta^{(2)}$ and $t^{(2)}$ using Eqs. (A6);
(6) An iterative process is used to determine $\beta^{(3)}$, using the relative energy of A11 and fcc;
(7) The hcp/fcc relative energy is used to determine $t^{(3)}$ using Eqs. (A7);
(8) The vacancy formation energy is used to determine $t^{(1)}$ using Eq. (A8);
(9) An iterative process is used to determine C_{min}, using the experimental value for the thermal expansion coefficient.

D. Computational details

The calculations presented below use either the molecular statics (MS) or the molecular dynamics (MD) technique. Typically the calculations for the solid (liquid) phases used a three-dimensional periodic cell of ~250 (4000) atoms with dynamic periodic boundaries.[20] The surface calculations used ~400 atoms in 2D geometry and had ~40 Å between the two free surfaces. The 0 K properties reported below are all relaxed with the maximum force <1 meV/Å. Temperature was controlled using a standard Nosé–Hoover thermostat[21,22] with a time constant of 0.1 ps. The quantities at temperature are thermodynamic averages for over at least 10 ps from samples that had been equilibrated at temperature and pressure for at least 10 ps. Statistical errors in energy are <10 meV/atom and in volume are <0.2 Å^3/atom. Average pressures were typically <100 MPa and average temperatures were typically within <1 K of the desired temperature. Errors in the temperature derivatives are estimated to be about 10%. The melting point was estimated using the moving interface method.[23] Using this estimate of temperature as a starting guess, microcanonical ensemble (N V E) runs of the two-phase slab geometry were run at a few different volumes, resulting in average temperatures of two-phase coexistence at different pressures. These average temperatures were interpolated to zero pressure resulting in the melting point. The error in melting point was assessed to be ±5°. The liquid structure factor was calculated as the Fourier transform of the radial distribution function, which was averaged over 20 configurations. The surface tension was approximated as the difference in potential energy between a liquid sphere of ~1000 atoms and the potential energy of an equivalent number of bulk liquid atoms at the same temperature, divided by the surface area of the sphere. Entropy differences were not calculated. When statistical errors are quoted in the text, the error represents one standard deviation determined from multiple runs.

The transport properties of liquid gallium presented below utilized Green–Kubo formalism.[24] In order to obtain meaningful statistical information for the transport properties we utilized the method of overlapped data collection.[25] A total of 2000 individual correlation functions were overlapped with a spacing of 0.1 ps. This choice allowed sufficient decay in the stress correlation function to not effect the results. The total length of the correlation function was 1 ps. The total length of the transport simulations was ~2 ns. The simulations used a microcanonical ensemble (N V E) of 1372 atoms with periodic boundaries such that the average pressure was zero. The energy conservation of the functions was excellent. The temperature fluctuations were <10 K and the pressure fluctuations were <800 bar. We estimate the statistical error in the self-diffusion coefficient to be <3% and the viscosity to be <8%.

III. RESULTS AND DISCUSSION

A. How the model compares to the first principles database

Using the GGA, the equilibrium cohesive energy, lattice constant, c_{11}, c_{12}, c_{44} and bulk modulus were calculated and

TABLE II. Quality of the fit quantities. Properties presented for the fcc structure are the lattice constant a, the elastic constants c_{ij}, the bulk modulus B which equals $(c_{11}+2c_{12})/2$, the second cubic shear c'_{12} which equals $(c_{11}-c_{12})/2$, the unrelaxed vacancy formation energy E^f_{iv}, and the force on an atom next to a vacancy f_v. Energies presented for the simple cubic structure $\Delta E_{\rm sc}$, the hcp structure $\Delta E_{\rm hcp}$, and the A11 structure $\Delta E_{\rm A11}$ are relative to the fcc structure. The volume per atom for the sc and hcp phases were held fixed at the fcc volume per atom. The A11 structure is completely relaxed. All of the MEAM quantities in this table were fit and are not predictions.

	MEAM	GGA
E_c (eV/atom)	2.897	2.897
a (Å)	4.247	4.247
c_{11} (GPa)	49	40
c_{12} (GPa)	54	59
c_{44} (GPa)	5	5
B (GPa)	53	52
c'_{12} (GPa)	−3	−10
E^f_{iv} (eV)	0.50	0.48
f_v (eV/Å)	−0.12	−0.13
$\Delta E_{\rm sc}$ (eV/atom)	0.067	0.068
$\Delta E_{\rm hcp}$ (eV/atom)	−0.013	−0.018
$\Omega_{\rm A11}$ (Å^3/atom)	19.39	20.15
$\Delta E_{\rm A11}$ (eV/atom)	−0.097	−0.043

are presented in Table II. The shear moduli c_{44} and $c'_{12}=0.5$ $(c_{11}$-$c_{12})$ are very small. These values are much smaller than those found in e.g., fcc-Al. In fact, $c'_{12}<0$ showing that the fcc phase is unstable with respect to a tetragonal distortion as seen by others.[26–28] The differences in the MEAM and GGA elastic constants are due to the fact that c'_{12} could not be fit exactly, as discussed above. The vacancy formation energy was calculated to be ~0.5 eV, which when compared to the melting point, is significantly higher than for other metals e.g., Al or Ni. The force on the neighboring atoms to the vacancy is calculated to be −0.12 eV/Å, where the sign is used to indicate that the force is directed radially toward the vacancy as is found in many other metals. The structural energies of sc, hcp, and A11 are also given in Table II. The sc and hcp volume per atom was held fixed at the volume per atom calculated for fcc. The c/a ratio for hcp was held at the ideal ratio. The A11 structure was completely relaxed.

The model is first exercised to calculate the properties that were used as input from the first principles calculations. The results are shown in Table II. All of these quantities for the fcc phase are derived from fully relaxed calculations at $T=0$ K and zero pressure except for the force on the atom next to the vacancy, which was calculated at constant volume and atom positions. The structural energies for sc and hcp were calculated at constant fcc volume and for A11 at zero pressure to mimic the GGA calculations. The agreement with the database is excellent in all cases except for the A11 energy that was a bit more stable than the GGA calculation and the c'_{12} elastic constant discussed above.

TABLE III. Predicted properties for gallium in the A11 structure. Quantities presented are cohesive energy E_c, atomic volume Ω, lattice constants a, b, c, internal coordinates x and z, and dimer bond length at 0 K. The thermal expansion coefficient CTE, anisotropy of thermal expansion $(\Delta L_i/L_i)/\Delta T$ for each direction i, and specific heat C_p are calculated at 300 K. The crystal structure parameters are based on an Abma analysis. Quoted statistical errors represent one standard deviation. Experimental values are for room temperature.

	MEAM	Experiment[a]	GGA
E_c (eV/atom)	−2.994[f]	−2.969	−2.940
Ω (Å^3/atom)	19.39[f]	19.47	20.15
a (Å)	4.82	4.52	4.569
b (Å)	4.53	4.51	4.564
c (Å)	7.11	7.64	7.731
x	0.067	0.079	0.083
z	0.167	0.153	0.156
Dimer bond length (Å)	2.456	2.444	2.529
CTE (10^{-6}/K)	58[g]	55	
$(\Delta L_a/L_a)/\Delta T$ (10^{-6}/K)	11±4	16.5,[b] 16.3,[c] 17.9[d]	
$(\Delta L_b/L_b)/\Delta T$ (10^{-6}/K)	10±6	11.5,[b] 3.7,[c] 9.0[d]	
$(\Delta L_c/L_c)/\Delta T$ (10^{-6}/K)	36±3	31.5,[b] 33.5,[c] 29.0[d]	
C_p (J/K mol)	24.9±0.1	25.8[e]	

[a]Reference 32.
[b]Reference 44.
[c]Reference 45.
[d]Reference 46.
[e]Reference 30.
[f]Fit to GGA.
[g]Fit to experiment.

B. How the model compares to experiment

The model is now used to calculate the properties of the equilibrium A11 and liquid phases. The results are presented in Tables III–V. The calculated cohesive energy and atomic volume for the A11 phase are in excellent agreement with experiment. The lattice constants vary slightly (~7%) from experiment, but their changes are in opposite directions, resulting in good agreement with the experimental volume. The internal atomic coordinates (x,z) are in excellent agreement with experiment and the predicted dimer length (2.455 Å) is within 1% of that seen in experiment (2.444 Å). For completeness the results of our GGA calculations for the A11 phase are also presented in Table III. For the A11 phase these GGA results give similar b/a and c/a ratios as previous LDA calculations by Bernasconi *et al.*,[29] but yield a volume much closer (+3%) to experiment than Bernasconi *et al.* (−9%). The coefficient of thermal expansion (CTE) has been fit to experiment and the quality of the fit is good. The anisotropic expansion behavior is correctly captured with the relative length changes in the crystal directions being in the order $c>a>b$. The statistical errors in the calculation of the anisotropic behavior are very large. The specific heat is in excellent agreement with experiment.[30]

The elastic constants are calculated at $T=0$ K by computing the second derivative of the energy with respect to specific distortions of the lattice. All elastic constants are posi-

TABLE IV. Predicted elastic constants for the A11 structure of gallium. Quantities presented are the bulk modulus B, the elastic constants c_{ij}, and the shear elastic constants $c'_{ij}=(0.5(c_{ii}+c_{jj})-c_{ij})/2$. Calculated values are for $T=0$ K, while the experimental values are for room temperature.

	MEAM (GPa)	Experiment[a] (GPa)
B	58	55,[b] 49[c]
c_{11}	74	100
c_{22}	97	90
c_{33}	78	135
c_{44}	14	35
c_{55}	11	42
c_{66}	22	40
c_{12}	53	37
c_{13}	30	33
c_{23}	65	31
c'_{12}	17	29
c'_{13}	16	42
c'_{23}	23	41

[a]Reference 32.
[b]Calculated from the experimental E and υ.
[c]GGA.

tive indicating that the A11 structure is stable (see Table IV). There is qualitative agreement with the experimental elastic constants measured at room temperature. For comparison, the calculated bulk modulus at $T=0$ K from GGA is 49 GPa.

The (001) surface energy and relaxations were also calculated. There are two possible surface terminations as discussed by Walko *et al.*[31] The A termination maintains the dimer bonds while the B termination splits the dimer bonds. The MEAM calculations give a relaxed surface energy of 0.83 (0.63) J/m^2 for the A (B) terminations. Thus the B termination is predicted to be favored in agreement with experiment. Surfaces with both terminations underwent significant atomic relaxation. For the B terminated surface the first three interplanar spacings are predicted to change by 2.0%, -0.2%, and 0.0% in poor agreement with the experimental relaxation of -9.6%, 10.2%, and -0.9%.

The liquid properties (Fig. 1) are in reasonable agreement with experiment. The calculated melting point of 367 ± 5 K is about 20% greater than experiment[32] (303 K). We found that by reducing $C_{\min}$ to 0.7 the calculated melting point was reduced to $\sim$320 K. Unfortunately at this $C_{\min}$, the thermal expansion coefficient for the A11 structure was nearly a factor of 2 greater than experiment. The predicted density [Fig. 1(a)] and its temperature derivative agree nicely with experiment.[33] The diffusivity [Fig. 1(b)] at high temperature is somewhat lower than experiment,[34] but the activation energy for diffusion (slope of the curve as plotted) is in reasonable agreement with experiment. The calculated viscosity [Fig. 1(c)] agrees nicely with experiment at high temperature,[33] but it increases more rapidly than experiment as the temperature is lowered. In Fig. 2 the specific heat is compared to experiment. The high temperature specific heat in the liquid compares quite favorably with experiment.[35] The temperature dependence of the specific heat in the liquid is in reasonable agreement with experiment, as may be seen

TABLE V. Properties for A11 to liquid transition in gallium. Quantities presented are the heat of fusion ΔH, the relative volume change on melting $\Delta V/V$, and the melting point T_m. The heat of fusion and volume change were calculated at 375 K.

	MEAM	Experiment[a]
ΔH (eV/atom)	0.063	0.058
$\Delta V/V$	-2.5%	-3.2%
T_m (K)	367 ± 5	303

[a]Reference 32.

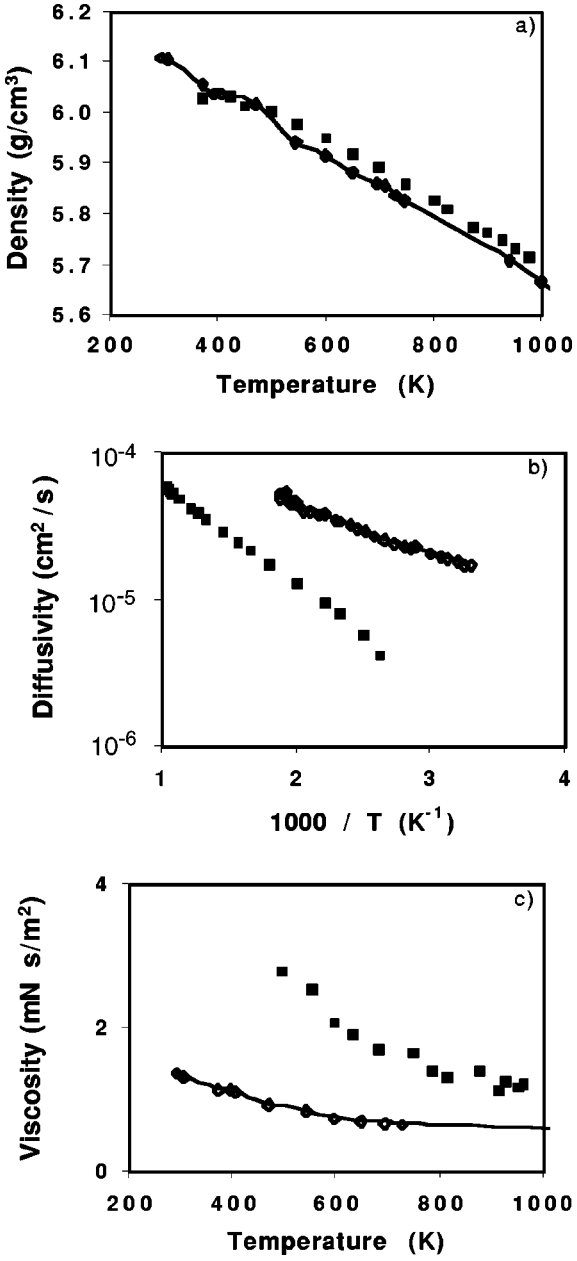

FIG. 1. Calculated (symbols) and experimental (Refs. 33 and 34) (line) values of density (a), diffusivity (b), and viscosity (c) of liquid Ga as a function of temperature.

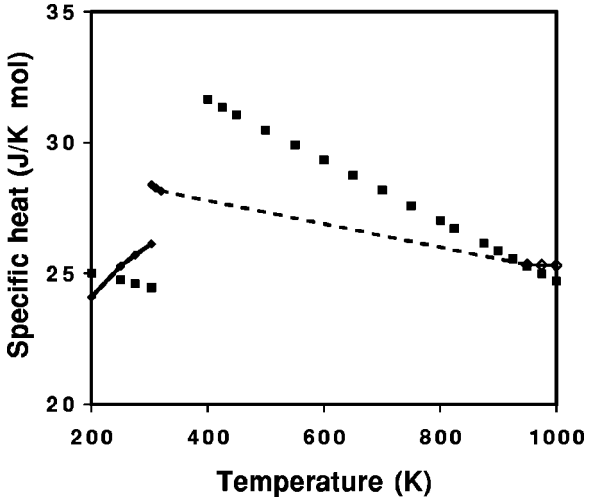

FIG. 2. Calculated (symbols) and experimental (Refs. 30 and 35) (line) values of the specific heat as a function of temperature.

by extrapolating (dotted line) the experimental high temperature specific heat to the low temperature specific heat of Amitin *et al.*[30] Similarly the solid specific heat agrees well with experiment[30] as noted above, even though the temperature dependence appears to be incorrect. The calculated approximate surface tension at 375 K of 0.55 J/m^2 is in reasonable agreement with the experimental value[32] of 0.72 J/m^2. Note that entropy effects were not included in the surface tension.

The structure factor $S(k)$ of liquid gallium has been studied extensively.[36–40] In Fig. 3(a) the calculated $S(k)$ for Ga at 375 K is presented. Except for the first peak, agreement with experimental[41] peak heights and positions measured at 325 K is excellent. The calculation shows a slight shoulder on the low-k side of the first peak in strong disagreement with the experiment, which shows a shoulder to the right of the first peak. Rapeanu and Padureanu[40] explain the split first peak by the existence of remnants of Ga–I (smaller k) and β-Ga (larger k) in the liquid. The relative heights of the two peaks depend on temperature and sample preparation. If this explanation is correct, then our simulation has a preponderance of the β-Ga in the liquid rather than the Ga–I seen in experiment. Gong *et al.*[38] relate the shoulder to the existence of short-lived dimers. Perhaps the dimer lifetime in the present calculations may be the cause of the disagreement with the experimental first peak. In Fig. 3(b) the pair correlation function $g(R)$ at 960 K is presented. The function shows a fairly broad peak first neighbor at ~2.8 Å and a very weak second neighbor peak at ~5.4 Å. For comparison the $g(R)$ extracted from experimental data[36] and a $g(R)$ from first principles[42] is shown. The peak positions are almost identical and the peak heights are very close to the MEAM calculation.

In Table V the properties of the melting transition of the A11 phase are given. The calculated latent heat of melting is about 8% greater than that found in experiment.[32] The MEAM calculation predicts that the A11 phase contracts upon melting in agreement with experiment.[32] The calculated contraction is about three-quarters of that seen in experiment. As noted above the calculated melting point is about 20% higher than experiment.

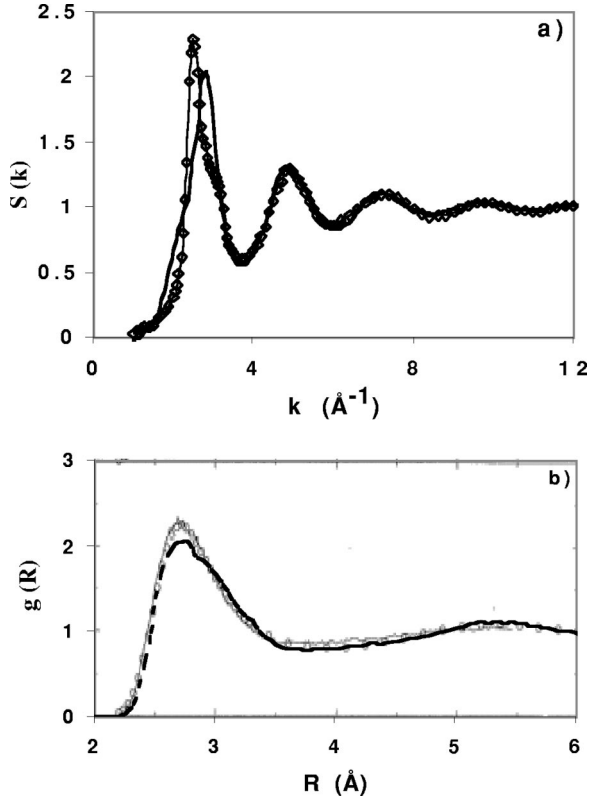

FIG. 3. Structure factor (a) for liquid Ga at 375 K for MEAM (line) and 325 K for experiment (Ref. 41) (symbols). Radial distribution function (b) for liquid Ga at 960 K for MEAM (dotted line) at 982 K for first principles (Ref. 42) (line) and at 959 K for experiment (Ref. 36) (symbols).

C. Structural stability

Since gallium undergoes a number of phase transformations under pressure, the MEAM model has been used to investigate the energy and volume per atom of a number of phases. The results are presented in Table VI. A few additional GGA calculations were performed to test the model and these results are also included in the table. It is quite satisfying to note that the A11 structure is predicted to be lower in energy than any of the other phases calculated. In addition, all of the experimentally observed phases, GaII, GaIII, GaIV, and β-Ga, are very close in energy to the A11 phase. Note that two equilibrium A20 (β-Ga) phases are found with different atomic volumes. The relative energy differences are all in reasonable agreement with the GGA calculations. In agreement with experiment, the A6 tetragonal distortion of the fcc phase is seen.

Note that the predicted atomic volume for the GaII is significantly lower than that of A11, hence high pressure favors its existence as observed in experiment. From the calculated energy vs volume the transition pressure is estimated to be ~7 GPa in good agreement with the experimental value of 5 GPa.[1] The predicted lattice constant at 2.6 GPa of 5.83 Å is about 2% smaller than that of 5.95 Å measured by Bosio.[43] Similarly, the predicted density for A6 (GaIII) of 6.33 g/cm^3 is about 4% below the experimental value of 6.57 g/cm^3 at 2.8 GPa.[43] The MEAM model predicts atomic vol-

TABLE VI. Energies, volumes, and bulk modulus of various structures at $T=0$ and zero pressure relative to the A11 (GaI) structure. Note two distinct A20 structures are found.

Structure				Energy (eV/atom)		Volume		Bulk modulus
Space group	Struktur-bericht	Pearson symbol	Common name	MEAM	GGA	MEAM	GGA	MEAM
63	A20	oC4	β-Ga[b]	0.007		1.008		0.97
220		cI12	GaII	0.062		0.854		1.08
227	A4	cF8	diamond	0.065	0.253	1.059	1.254	0.92
63	A20	oC4	β-Ga[b]	0.077		0.904		1.00
194	A3	hP2	hcp	0.080	0.056	0.957	0.950	0.91
141	A5	tI4	β-Sn	0.089		0.823		1.13
139	A6[a]	tF4	fct-GaIII	0.090	0.030	0.959	0.949	0.90
229	A2	cI2	bcc	0.095	0.051	0.872	0.966	1.01
225	A1	cF4	fcc-GaIV	0.097	0.043	0.953	0.950	0.91
221	A_h	cP1	simple cubic	0.134	0.091	0.862	1.007	1.06
194	A9	hP4	graphite	0.202		1.024		0.88

[a]fct (tF4) and bct (tI2) are the same structure.
[b]oC4 and mC4 (space group 15) are essentially the same structure.

umes for the fcc and hcp phases to be only slightly less (95%) than the A11 atomic volume, in excellent agreement with the GGA calculations. For bcc and sc, MEAM predicts atomic volumes significantly smaller than the GGA prediction. A summary of the MEAM and GGA results for the hcp structure is given in Table VII. For the hcp structure the GGA (MEAM) predicts a c/a ratio of 1.64 (1.45). The first-principles calculation gives a c/a ratio slightly greater than the ideal ratio, while MEAM gives a value significantly less than ideal. It is an intrinsic property of a first neighbor MEAM model that the c/a ratio is less than ideal for a material in which the hcp structure is more stable than the fcc structure.

IV. SUMMARY

An atomic level MEAM model for Ga has been developed. Using predominantly input from GGA calculations, the parameters of the MEAM potential were determined. The model agrees quite well with the GGA database. By testing the potential for both solid and liquid phases, it was determined that the model represents many properties of Ga in close agreement with experiment. Notable exceptions include the c/a ratio, a few elastic constants, and the (001) surface relaxation for the A11 phase, and the first peak of the liquid structure factor. Properties investigated include phase stability and geometry at ambient pressure, elastic constants, thermal expansion, specific heat, diffusivity, viscosity, free surface stability and relaxation, and melting point.

TABLE VII. Predicted properties of the hcp phase of gallium. Quantities presented are the lattice constant a, c/a ratio, and bulk modulus B.

	MEAM	GGA
a (Å)	3.13	2.996
c/a	1.45	1.644
B (GPa)	53	48

APPENDIX

A number of detailed equations are collected here for the convenience of the reader. The partial electron densities used in Eq. (9) are given by the following equations:

$$(\overline{\rho}^{(1)})^2=\sum_{\alpha}\left[\sum_{j(\neq i)}\frac{R_{ij}^{\alpha}\rho^{a(1)}(R_{ij})}{R_{ij}}\right]^2, \tag{A1}$$

$$(\overline{\rho}^{(2)})^2=\sum_{\alpha,\beta}\left[\sum_{j(\neq i)}\frac{R_{ij}^{\alpha}R_{ij}^{\beta}\rho^{a(2)}(R_{ij})}{R_{ij}^2}\right]^2 - \frac{1}{3}\left[\sum_{j(\neq i)}\rho^{a(2)}(R_{ij})\right]^2, \tag{A2}$$

$$(\overline{\rho}^{(3)})^2=\sum_{\alpha,\beta,\gamma}\left[\sum_{j(\neq i)}\frac{R_{ij}^{\alpha}R_{ij}^{\beta}R_{ij}^{\gamma}\rho^{a(3)}(R_{ij})}{R_{ij}^3}\right]^2 - \frac{3}{5}\sum_{\alpha}\left[\sum_{j(\neq i)}\frac{R_{ij}^{\alpha}\rho^{a(3)}(R_{ij})}{R_{ij}}\right]^2, \tag{A3}$$

where R_{ij}^{α} is the projection of R_{ij} in the α-direction. The atomic electron densities used in to calculate the partial electron densities are given by

$$\rho^{a(l)}(R)=e^{-[\beta^{(l)}(R/r_e)-1]}. \tag{A4}$$

The force on the first neighbor of a vacancy is given by

$$f_v = \frac{AE_c}{r_e Z}\left\{ -\beta^{(0)} + \frac{1}{Z\overline{\rho}_v}\left[1+\ln\left(\frac{\overline{\rho}_v}{Z}\right)\right]\sum_{l=0}^{3} t^{(l)}(v^l + w^l\beta^{(l)})\right\}, \tag{A5a}$$

$$\overline{\rho}_v = \sqrt{(Z-1)^2 + t^{(1)} + \tfrac{2}{3}t^{(2)} + \tfrac{2}{5}t^{(3)}}, \tag{A5b}$$

where $v^1=0$, 60, -6, -9 and $w^1=132$, -48, 10, 7.8 for $l=0$, 3 respectively, and $\overline{\rho}_v$ is the background electron density at the vacancy (see Baskes *et al.*[11] for details).

The equations for the shear elastic constants used to determine $\beta^{(2)}$ and $t^{(2)}$ are given by

$$c_{44} = \frac{E_c}{\Omega}\left[\frac{\alpha^2 - A{\beta^{(0)}}^2}{Z} + \frac{2At^{(2)}(\beta^{(2)}-2)^2}{Z^2}\right], \tag{A6a}$$

$$\frac{c_{11}-c_{12}}{2} = \frac{E_c}{\Omega}\left[\frac{\alpha^2 - A{\beta^{(0)}}^2}{2Z} + \frac{At^{(2)}(\beta^{(2)}-6)^2}{2Z^2}\right]. \tag{A6b}$$

The equation for the hcp energy used to determine $t^{(3)}$ is

$$\Delta E_{\rm hcp} = F(\overline{\rho}_{\rm hcp}/Z), \tag{A7a}$$

where

$$\overline{\rho}_{\rm hcp} = \sqrt{Z^2 + \tfrac{1}{3}t^{(3)}}. \tag{A7b}$$

The equation for the vacancy formation energy used to determine $t^{(1)}$ is

$$E_{1v}^f = E_c + ZF(\overline{\rho}_v/Z), \tag{A8}$$

where $\overline{\rho}_v$ is given above in Eq. (A5b).

Screening of atoms i and k by an atom j was implemented using the angular screening technique first described by Baskes *et al.*[18] Both the pair potential and the atomic electron densities are screened by the factor given by

$$S_{ik} = \prod_{j\neq i,k} S_{ijk}. \tag{A9a}$$

Consider the ellipse drawn through the three atoms. The equation of the ellipse is captured by the parameter C,

$$x^2 + \frac{y^2}{C} = \left(\frac{R_{ik}}{2}\right)^2, \tag{A9b}$$

where

$$C = \frac{2(X_{ij}+X_{jk}) - (X_{ij}-X_{jk})^2 - 1}{1-(X_{ij}-X_{jk})^2} \tag{A9c}$$

and

$$X_{ij} = \left(\frac{R_{ij}}{R_{ik}}\right)^2; X_{jk} = \left(\frac{R_{jk}}{R_{ik}}\right)^2. \tag{A9d}$$

There are two limiting ellipses captured by the parameters $C_{\rm min}$ and $C_{\rm max}$. For atom j outside the outer ellipse, $C > C_{\rm max}$, $S_{ijk}=1$ and the ij interactions are completely unscreened. Similarly for atom j inside the inner ellipse, $C < C_{\rm min}$, $S_{ijk}=0$ and the ij interactions are completely screened. For intermediate C an interpolation function is used,

$$S_{ijk} = \left[1 - \left(\frac{C_{\rm max}-C}{C_{\rm max}-C_{\rm min}}\right)^4\right]^2. \tag{A9e}$$

[1] O. Schulte and W. B. Holzapfel, Phys. Rev. B **55**, 8122 (1997).
[2] R. Ravelo and M. Baskes, Phys. Rev. Lett. **79**, 2482 (1997).
[3] M. I. Baskes, Phys. Rev. B **62**, 15 532 (2000).
[4] M. S. Daw and M. I. Baskes, Phys. Rev. Lett. **50**, 1285 (1983).
[5] M. S. Daw and M. I. Baskes, Phys. Rev. B **29**, 6443 (1984).
[6] M. S. Daw, S. M. Foiles, and M. I. Baskes, Mater. Sci. Rep. **9**, 251 (1993).
[7] M. I. Baskes, Phys. Rev. B **46**, 2727 (1992).
[8] M. I. Baskes, Phys. Rev. Lett. **59**, 2666 (1987).
[9] M. I. Baskes, J. S. Nelson, and A. F. Wright, Phys. Rev. B **40**, 6085 (1989).
[10] J. H. Rose, J. R. Smith, F. Guinea, and J. Ferrante, Phys. Rev. B **29**, 2963 (1984).
[11] M. I. Baskes, M. Asta, and S. G. Srnivasan, Philos. Mag. A **81**, 991 (2001).
[12] M. I. Baskes, Mater. Sci. Eng., A **261**, 165 (1999).
[13] D. Vanderbilt, Phys. Rev. B **41**, 7892 (1985).
[14] J. P. Perdew, Physica B **172**, 1 (1991).
[15] G. Kresse and J. Hafner, Phys. Rev. B **47**, 558 (1993).
[16] G. Kresse and J. Hafner, Phys. Rev. B **49**, 14 251 (1994).
[17] H. J. Monkhorst and J. D. Pack, Phys. Rev. B **13**, 5188 (1976).
[18] M. I. Baskes, J. E. Angelo, and C. L. Bisson, Modell. Simul. Mater. Sci. Eng. **2**, 505 (1994).
[19] M. I. Baskes, Mater. Chem. Phys. **50**, 152 (1997).
[20] M. Parrinello and A. Rahman, J. Appl. Phys. **52**, 7182 (1981).
[21] W. G. Hoover, Phys. Rev. A **31**, 1695 (1985).
[22] S. Nose, Prog. Theor. Phys. Suppl. **103**, 1 (1991).
[23] M. I. Baskes, Phys. Rev. Lett. **83**, 2592 (1999).
[24] D. A. McQuarrie, *Statistical Mechanics* (University Science Books, Sausalito, 2000).
[25] D. C. Rapaport, *The Art of Molecular Dynamics Simulation* (Cambridge University Press, Cambridge, 1995).
[26] T. Kenichi, K. Kazuaki, and A. Masao, Phys. Rev. B **58**, 2482 (1998).
[27] S. I. Simak, U. Haussermann, R. Ahuja, S. Lidin, and B. Johansson, Phys. Rev. Lett. **85**, 142 (2000).
[28] Z. Li and J. S. Tse, Phys. Rev. B **62**, 9900 (2000).
[29] M. Bernasconi, G. L. Chiarotti, and E. Tosatti, Phys. Rev. B **52**, 9988 (1995).
[30] E. B. Amitin, Y. F. Minenkov, O. A. Nabutovskaya, I. E. Paukov, and S. I. Sokolova, J. Chem. Thermodyn. **16**, 431 (1984).
[31] D. A. Walko, I. K. Robinson, C. Grütter, and J. H. Bilgram, Phys. Rev. Lett. **81**, 626 (1998).
[32] E. A. Brandes, in *Smithells Metals Reference Book* (Butterworths, London, 1983).

[33] H. v. Tippelskirch, Ber. Bunsenges. Phys. Chem. **80**, 726 (1976).
[34] H. Riedl, T. Persgon, and P.-E. Eriksson, Int. J. Appl. Radiat. Isot. **30**, 481 (1979).
[35] S. N. Banchila, D. K. Palchaev, and L. P. Filippov, High Temp. **17**, 426 (1979).
[36] M. C. Bellissent-Funel, P. Chieux, D. Levesque, and J. J. Weis, Phys. Rev. A **39**, 6310 (1989).
[37] A. D. Cicco and A. Filipponi, J. Non-Cryst. Solids **156–158**, 102 (1993).
[38] X. G. Gong, G. L. Chiarotti, M. Parrinello, and E. Tosatti, Europhys. Lett. **21**, 469 (1993).
[39] A. H. Shinohara, K. Omote, Y. Waseda, and J. M. Toguri, High Temp. Mater. Proc. **15**, 237 (1996).
[40] S. N. Rapeanu and I. Padureanu, Phys. Scr., T **T57**, 18 (1995).
[41] Y. Waseda, *The Structure of Non-Crystalline Materials* (McGraw–Hill, New York, 1980).
[42] J. M. Holender, M. J. Gillan, M. C. Payne, and A. D. Simpson, Phys. Rev. B **52**, 967 (1995).
[43] L. Bosio, J. Chem. Phys. **68**, 1221 (1978).
[44] M. Yaqub and J. Cochran, Phys. Rev. **137**, A1182 (1965).
[45] C. S. Barrett, *Advances in X-Ray Analysis* (Plenum, New York, 1962).
[46] E. I. Geshko, V. P. Mikhal'chenko, and B. M. Sharlai, Sov. Phys. Solid State **14**, 1554 (1972).